journal

J. Am. Ceram. Soc., 97 [3] 798–804 (2014)
DOI: 10.1111/jace.12676

Strengthening of Thermoelectric Performance via Ir Doping in Layered $Ca_3Co_4O_9$ System

Yanan Huang,[‡] Bangchuan Zhao,[‡,†] Shuai Lin,[‡] Ran Ang,[‡] Wenhai Song,[‡] and Yuping Sun[‡,§,¶,†]

[‡]Key Laboratory of Materials Physics, Institute of Solid State Physics, Chinese Academy of Sciences, Hefei 230031, China

[§]High Magnetic Field Laboratory, Chinese Academy of Sciences, Hefei 230031, China

[¶]University of Science and Technology of China, Hefei 230026, China

The effects of Ir doping on thermoelectric (TE) as well as transport and magnetic properties of $Ca_3Co_{4-x}Ir_xO_9$ ($0 \le x \le 0.4$) series samples have been investigated systematically. Based on the analysis of X-ray photoelectron spectroscopy data, the valence state of the doped Ir ions is suggested to be +4. As Ir ions are doped into system, both the resistivity and the metal-insulator transition temperature increase till to $x = 0.3$, indicating the more stable spin-density-wave state in these Ir-doped samples. The thermopower increases monotonously with increasing x. For $x = 0.4$ sample, its room-temperature thermopower S_{300K} reaches 166.2 μV/K, which is 36% larger than that of the undoped sample. The results show that a proper Ir doping may be an effective route to strengthen the TE performance of $Ca_3Co_4O_9$ system, which is suggested to originate from the variations of carrier concentration and lattice disharmony induced by Ir doping. At the same time, Ir doping suppresses the low-temperature ferrimagnetic state and also introduces a spin-glass behavior at low temperatures.

I. Introduction

THERMOELECTRIC (TE) materials have attracted much attention because they could be utilized to generate electricity directly making use of waste heat.[1,2] A practical TE material should have high efficiency, which is characterized by the dimensionless TE figure of merit ZT ($=S^2T/\rho\kappa$, where S, T, ρ, and κ are thermopower, absolute temperature, electrical resistivity, and thermal conductivity, respectively.).[3,4] As the discovery of good TE performance in $Na_xCo_2O_4$ ($NaCo_2O_4$),[5] Ca–Co–O,[6,7] $Bi_2Sr_2Co_2O_y$,[8] and Tl–Sr–Co–O,[9] these layered cobalt oxides have been the object with a regained attention.[10] In this cobaltite family, the so-called $Ca_3Co_4O_9$ occupies a special place,[6,11] where the coexistence of metallic transport behavior and high thermopower makes it suitable as a potential candidate of TE materials, especially in an oxidation condition.[12,13]

Usually, $Ca_3Co_4O_9$ can be embodied as $[Ca_2CoO_3]_{0.62}[CoO_2]$, which composes of two subsystems stacking alternately along the c-axis: the rock-salt-type Ca_2CoO_3 (CaO–CoO–CaO) layers and the CdI_2-type CoO_2 layers.[6] Both subsystems have monoclinic crystal symmetry ($C_{2/m}$), which have identical a, c, and β but different b parameters, resulting in the structural misfit along b-axis.[5,9,10] Due to its misfit-layered structure, except for TE performance, a few of transport and magnetic characteristics have also been observed in $Ca_3Co_4O_9$ system, such as, the metal-insulator transition (MIT), the incommensurate spin density wave (IC-SDW) ordering, and the ferrimagnetic (FIM) state, etc.[6,13]

For the sake of improving the TE performance of $Ca_3Co_4O_9$ system, the study of element substitution at Co sites is a very important route due to the multivalence of Co ions in the material. So far, for $Ca_3Co_4O_9$ system, the doping effect at Co sites has been extensively investigated and is mainly focused on the 3d transition-metal elements, such as, Ti,[14,15] Cr,[12,16] Mn,[10] Fe,[10,12,16] Ni,[16] Cu,[10,17] and Zn.[16] Compared with these 3d transition-metal elements, the doping of 5d ones, such as Ir doping, has not been investigated systematically and may be more beneficial to the TE performance of $Ca_3Co_4O_9$ system. Similar expectation has already been achieved in a series samples. For example, in $PtSb_2$ system, a pronounced enhancement of TE performance has been induced by Ir doping.[2] In this article, we report a systematic study of electrical and thermal transport as well as magnetic properties on $Ca_3Co_{4-x}Ir_xO_9$ ($0 \le x \le 0.4$) series samples. We find that a proper Ir doping is effective to improve the TE performance of $Ca_3Co_4O_9$ system.

II. Experimental Procedure

Polycrystalline samples of $Ca_3Co_{4-x}Ir_xO_9$ ($x = 0$, 0.1, 0.2, 0.3, and 0.4) were prepared by the solid-state reaction method. High-purity $CaCO_3$ (99.95%; Alfa-Aesar, Ward Hill, MA), Co_3O_4 (99.9985%; Alfa-Aesar), and IrO_2 (99.99%; Alfa-Aesar) powders were thoroughly mixed according to the desired stoichiometry in the molar ratio Ca: Co: Ir = 3: $(4-x)$: x, and prefired at 1173 K for 24 h twice with an intermediate grinding for 30 min in air. And then, the obtained mixtures were reground for 30 min, pressed into 11.5 mm diameter dish-shaped pellets, and sintered at 1173 K for 24 h in air to obtain homogeneous samples.

The composition of the samples was analyzed by the energy dispersive spectroscopy (EDS) technique. The structure and the micrograph of the samples were examined by the powder X-ray diffraction (XRD) using a Philips X' pert PRO X-ray diffractometer (XRD, PANalytical B.V., Almelo, the Netherlands) with CuK_α radiation and a scanning electron microscope (SEM) at room temperature. Rietveld refinement was performed on the XRD data using JANA 2006 program.[20,21] The valence state of relevant ions was determined by the X-ray photoelectron spectroscopy (XPS) technique using AlK_α radiation at room temperature. The electrical and thermal transport properties measurements were performed on a physical property measurement system (PPMS-9T) using the four- or five- (Hall measurement) probe method. The sample dimensions are about 3 mm × 1.8 mm × 1.2 mm, 5 mm × 2 mm × 1.2 mm, and 2 mm × 2 mm × 0.5 mm for the electrical transport, thermal transport, and Hall measurements, respectively. The

M. A. White—contributing editor

Manuscript No. 33293. Received June 3, 2013; approved September 29, 2013.
†Authors to whom correspondence should be addressed. e-mails: bchzhao@issp.ac.cn and ypsun@issp.ac.cn

magnetic properties were measured on a superconducting quantum interference device (SQUID) measurement system (MPMS-5T).

III. Results and Discussions

(1) Structure

The room-temperature XRD patterns of $Ca_3Co_{4-x}Ir_xO_9$ (x = 0, 0.1, 0.2, 0.3, and 0.4) samples are shown in the main panel of Fig. 1(a). All are single phase and in agreement with the previously reported data for $Ca_3Co_4O_9$ structure.[6,22] However, as the Ir-doping level is greater than 0.4, such as x = 0.45, a small impurity phase of $Ca_3Co_2O_6$ appears in the XRD pattern, meaning that the solubility of Ir in $Ca_3Co_4O_9$ system is about 0.4. Figure. 1(b) shows the XPS result for Ir ions. It can be seen that the binding energy of the fitted Ir $4f_{7/2}$ peak locates on ~63.7 eV, indicating that Ir ions enter into $Ca_3Co_4O_9$ system in the form of Ir^{4+}.

To show the effect of Ir doping on the lattice clearly, the enlarged (002) peaks are shown in Fig. 1(c) for all studied samples. It displays that, as Ir-doping content x increases, the peaks move to a lower angle position. Figure. 1(d) shows the Rietveld refinement of XRD data on $Ca_3Co_{3.6}Ir_{0.4}O_9$ as an example. The super-space group $X2/m(0b0)s0$ is employed in such a refinement for all samples[23,24] and the refined lattice parameters are given in Table I. From Table I, we can see that the lattice parameters a, b_1, b_2, and c increase simultaneously with increasing x.

Table II gives the EDS analysis results for $Ca_3Co_{4-x}Ir_xO_9$ (x = 0, 0.1, 0.2, 0.3, and 0.4) samples. It could be found that the real contents of the three kinds of ions in these samples are almost the same with that of the nominal one. The content of Ca ions almost keeps unchanged, whereas the content of Co ions decreases monotonously with increasing x. It should be noted that the oxygen content is also a key parameter to affect the physical properties of $Ca_3Co_4O_9$ system. The substitution of Co ions by Ir^{4+} is considered to reduce the average valance state of Co ions or introduce additional

Table I. Lattice Parameters a, b_1, b_2, c, and β for the $Ca_3Co_{4-x}Ir_xO_9$ (x = 0, 0.1, 0.2, 0.3, and 0.4) Samples. Here, b_1 and b_2 are the b-axis lengths for $[Ca_2CoO_3]$ and $[CoO_2]$ Subsystems, Respectively

x	a(Å)	b_1(Å)	b_2(Å)	c(Å)	β(°)
0	4.8260(5)	4.5309(7)	2.8101(2)	10.8243(2)	97.7862(1)
0.1	4.8266(1)	4.5323(4)	2.8110(3)	10.8308(6)	98.0169(2)
0.2	4.8339(0)	4.5549(5)	2.8268(6)	10.8365(7)	98.2671(1)
0.3	4.4446(6)	4.5631(3)	2.8402(0)	10.8379(2)	98.3078(2)
0.4	4.8502(1)	4.5740(6)	2.8472(1)	10.8394(1)	98.3221(2)

O ions. However, for the present samples, all samples are prepared using the same processing parameters as described above, which may lead to the only subtle oxygen variation. It has been observed that the oxygen stoichiometry in $Ca_3Co_4O_9$ samples is only changed by 2% even the annealing atmosphere is changed from oxygen (90-atm-O^2) to air. So, we can assume in nature that the oxygen content in present samples is almost the same due to the same processing parameters.[18] Furthermore, the change in the oxygen content will induce the variation in the relative physical properties. As reported previously, the room-temperature carrier concentration n_{300K} will increase as the oxygen content increases, simultaneously the c-axis structural parameter d_c, MIT temperature T_{min}, room-temperature resistivity ρ_{300K} and thermopower S_{300K} will decrease in both polycrystalline and single-crystal $Ca_3Co_4O_9$ samples.[18,19] However, in our present samples, n_{300K} decreases, d_c, T_{min}, ρ_{300K}, and S_{300K} increase as Ir ions are doped into the system as discussed below. The obtained results show that the role of the variation in oxygen content in the determination of physical properties is weaker compared with that of Ir doping and the variation in the relative physical properties is mainly induced by the substitution effect of Ir ions for Co in the $Ca_3Co_4O_9$ lattice.

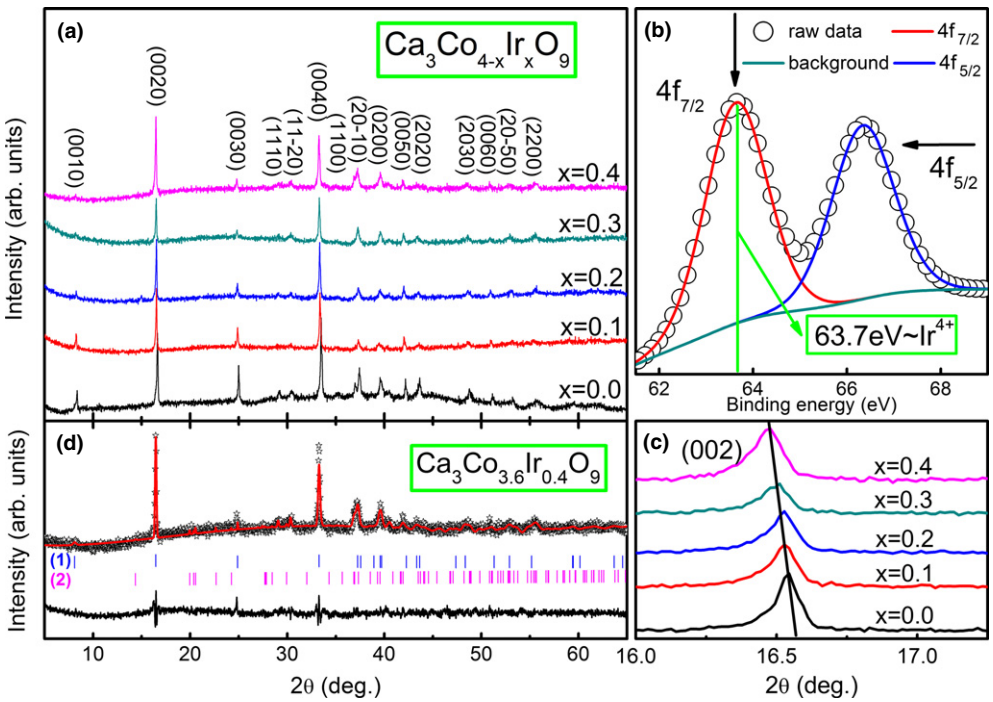

Fig. 1. (a) X-ray diffraction (XRD) patterns of $Ca_3Co_{4-x}Ir_xO_9$ (x = 0, 0.1, 0.2, 0.3, and 0.4); (b) the X-ray photoelectron spectroscopy result for Ir ions; (c) the enlarged (002) peaks for all samples; (d) Rietveld refinement of XRD data on $Ca_3Co_{3.6}Ir_{0.4}O_9$, the observed (cross), calculated (solid red line), and difference (bottom black line) profiles are shown, the bars show the peak positions of reflections common to both subsystems (1) and satellite reflections (2).

Table II. Nominal and Real Composition of the $Ca_3Co_{4-x}Ir_xO_9$ (x = 0, 0.1, 0.2, 0.3, and 0.4) Samples Determined by EDS Analysis

Samples	Ca/f.u.	Co/f.u.	Ir/f.u.
$Ca_3Co_4O_{9-\delta}$	2.989	4.011	0
$Ca_3Co_{3.9}Ir_{0.1}O_{9-\delta}$	3.009	3.896	0.095
$Ca_3Co_{3.8}Ir_{0.2}O_{9-\delta}$	2.983	3.822	0.185
$Ca_3Co_{3.7}Ir_{0.3}O_{9-\delta}$	3.019	3.702	0.279
$Ca_3Co_{3.6}Ir_{0.4}O_{9-\delta}$	3.013	3.607	0.380

Combining with the results of XPS, XRD, EDS and considering the standard ionic radius of Ir^{4+} (0.625 Å), which is closer to that of Co^{3+} (0.545 Å) and is larger than it, we speculate that Ir ions may mostly enter into Co^{3+} sites of both subsystems in $Ca_3Co_4O_9$ lattice and the corresponding lattice parameters a, b_1, b_2, and c are expanded systematically.

Figures 2(a)–(c) illustrate the SEM images of the surfaces for the $Ca_3Co_{4-x}Ir_xO_9$ samples with x = 0, 0.2, and 0.4, respectively, as examples. Plate-like crystal grains can be observed clearly in the figures, which is the nature of the layered crystal structure for $Ca_3Co_4O_9$ system.[7] Such a nature is exhibited more clearly in Fig. 2(d), where the enlarged SEM image of the surface for the x = 0.2 sample is shown. With increasing x, the crystal grains become smaller and more homogeneous gradually. The smaller grain size and lower textured structure will suppress the carrier transport due to the increased grain boundary and thus will decrease carrier mobility μ as shown in the inset of Fig. 4.

The bulk density was measured by applying Archimedes principle at room temperature. The obtained density values are 3.75, 3.83, 3.94, 3.92, and 4.08 g/cm^3 for the samples with x = 0, 0.1, 0.2, 0.3, and 0.4, respectively, which are about 76%–82% of that of theoretical fully dense material (4.94 g/cm^3). These values are mainly in agreement with an earlier report.[10] Wang *et al.*[10] have reported that the bulk density of samples is in the range ~3.8–3.9 g/cm^3, this value is 78% of theoretical density. Moreover, we could see that the bulk density of the studied samples almost increases monotonously with increases x.

(2) Electrical Transport Properties

The temperature dependence of resistivity $\rho(T)$ for $Ca_3Co_{4-x}Ir_xO_9$ (x = 0, 0.1, 0.2, 0.3, and 0.4) samples is shown in the main panel of Fig. 3. All samples with $x \leq 0.3$ show a similar transport behavior: semiconducting behavior below T_{min} and metallic behavior above T_{min}. That is to say, there exists a minimum around T_{min} in $\rho(T)$ curves for these samples, which is suggested to originate from the formation of the IC-SDW state.[25] The charge carriers will be localized by the emergence of IC-SDW ordering, giving rise to the MIT.[10] As x increases, the MIT temperature T_{min} shifts to the higher temperatures as shown in the inset of Fig. 3, indicating that the SDW state becomes more stable in these Ir-doped samples. Such a phenomenon may originate from the enhanced random Coulomb potential, which is caused by the disorder effect due to the introduction of Ir ions with a larger ionic radius into $Ca_3Co_4O_9$ lattice. For the sample with x = 0.4, no MIT exists in $\rho(T)$ curve and it behaves as a semiconductor in the whole measured-temperature range.

To understand the effect of Ir doping on the variation in electrical transport properties, the semiconducting $\rho(T)$ data below T_{min} are fitted by the thermally activated conduction model[10,14,26]: $\rho^{-1}(T) = \mu(T)\exp(-E_0/k_BT)$ as shown in the main panel of Fig. 4. Here, μ is the carrier mobility, E_0 is the energy gap resulting from the SDW at the Fermi surface, and k_B is the Boltzmann constant. The obtained thermally active energy E_0 are 0.7, 1.2, 2.0, 5.9, and 16.1 meV for the samples with x = 0, 0.1, 0.2, 0.3, and 0.4, respectively. The monotonously increased E_0 with increasing x indicates that the carriers need more energy to be excited due to the more stable SDW state induced by Ir doping. The results are in good coherence with the increased T_{min} for the samples with $x \leq 0.3$ as discussed above. When x reaches 0.4, E_0 becomes so large and the carrier localization becomes so strong that the MIT is suppressed completely.

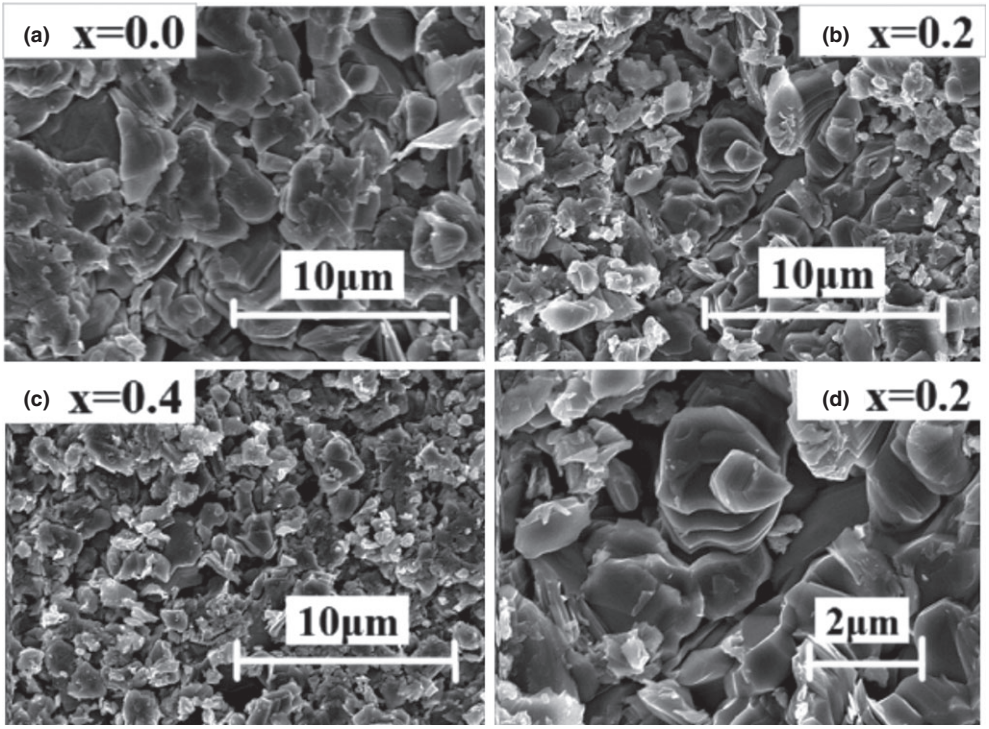

Fig. 2. (a)–(c) Scanning electron microscope (SEM) micrographs for the $Ca_3Co_{4-x}Ir_xO_9$ samples with x = 0, 0.2, and 0.4, respectively; (d) enlarged SEM micrograph for the x = 0.2 sample.

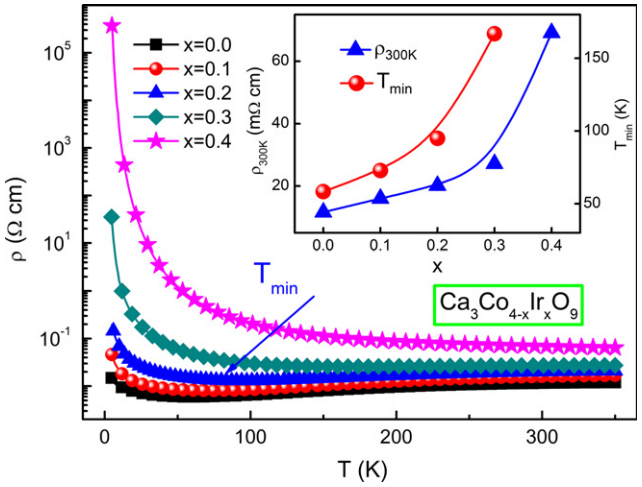

Fig. 3. Temperature dependence of resistivity $\rho(T)$ for $Ca_3Co_{4-x}Ir_xO_9$ (x = 0, 0.1, 0.2, 0.3, and 0.4), here the arrow denotes the metal-insulator transition temperature T_{min}, the inset shows the T_{min} and the room-temperature resistivity ρ_{300K} as functions of Ir-doping content x.

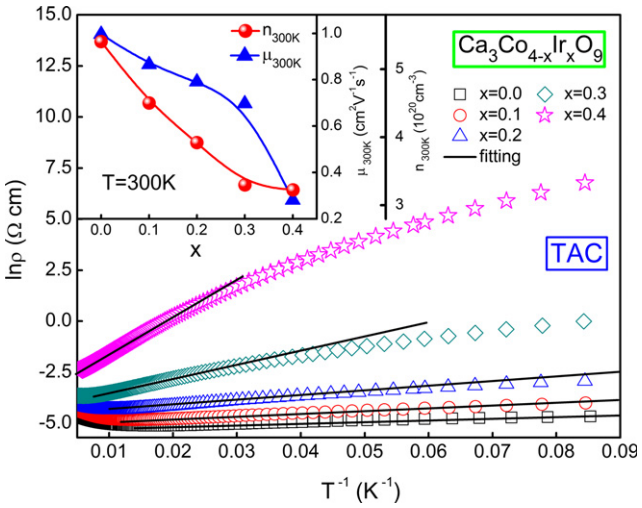

Fig. 4. Plots of lnρ against T^{-1} with the fitted lines for $Ca_3Co_{4-x}Ir_xO_9$ (x = 0, 0.1, 0.2, 0.3, and 0.4), the inset shows the room-temperature carrier concentration n_{300K} and mobility μ_{300K} as functions of Ir-doping content x.

From the main panel of Fig. 3, we can also see that the magnitude of the resistivity increases monotonously with increasing x in the full investigated temperature range. The quantitative description of the resistivity change can be seen clearly in the inset of Fig. 3, where the Ir-doping content dependence of the room-temperature resistivity ρ_{300K} is plotted as an example. To study the physical origin of the resistivity variation, we performed Hall resistivity $\rho_{xy}(H)$ measurement at room temperature for all samples. The room-temperature carrier concentration n_{300K} calculated from the measured $\rho_{xy}(H)$ is shown in the inset of Fig. 4. It is well-known that, in $Ca_3Co_4O_9$ system, majority of carriers are hole, and the average valence of Co ions is about +3 depending on the oxygen content.[10] By doping, the carriers can vary over a remarkably wide range so that the effective valence of Co ions changes from Co^{4+} to Co^{2+} in this material.[10] As the change in oxygen content is slight, the valence of Ir^{4+} is higher than the average valence of Co ions in $Ca_3Co_4O_9$ system.[27] Consequently, the substitution of Ir^{4+} for Co ions in both subsystems can be considered as "electron-doping" like and can introduce additional electrons into the system, which will decrease the relative concentration of

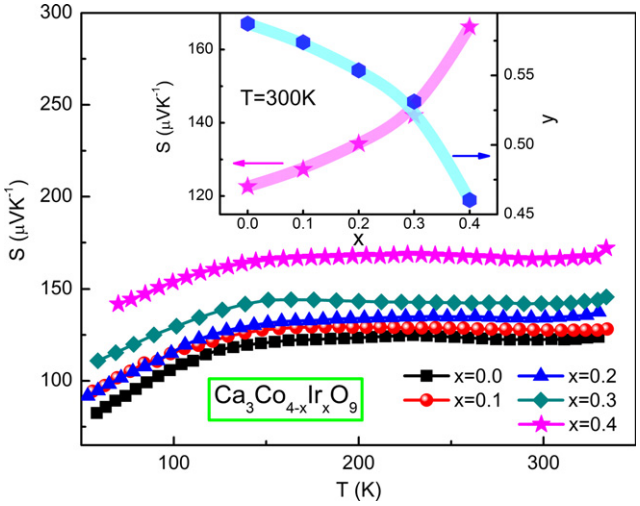

Fig. 5. Temperature dependences of thermopower $S(T)$ for $Ca_3Co_{4-x}Ir_xO_9$ (x = 0, 0.1, 0.2, 0.3, and 0.4), the inset shows the room-temperature thermopower S_{300K} and the calculated Co^{4+} concentration y as functions of Ir-doping level x.

Co^{4+} ions and increase that of Co^{2+}. Thus, n_{300K} decreases monotonously with increasing x as shown in the inset of Fig. 4. Moreover, the scattering for carriers enhances due to the enhanced disorder effect induced by Ir doping with a larger ionic radius in the conductive CoO_2 layers, which leads to the decrease in the room-temperature carrier mobility μ_{300K}, especially for the x = 0.4 sample as plotted in the inset of Fig. 4. The combined effect of the decreased n_{300K} and μ_{300K} results in the gradual increase in ρ_{300K} according to equation[28]: $\rho^{-1} = ne\mu$ via Ir doping.

(3) Thermoelectric Properties

The main panel of Fig. 5 shows the temperature dependence of the thermopower $S(T)$ for $Ca_3Co_{4-x}Ir_xO_9$ (x = 0, 0.1, 0.2, 0.3, and 0.4) samples. The positive value of S demonstrates the majority of the charge carriers are hole-type. In addition, all $S(T)$ curves strongly depend on T below 150 K, while they exhibit a almost T-independent behavior above 200 K. The Ir doping can boost S considerably in the full investigated-temperature region, especially for the heavy Ir-doping content. To describe such a phenomenon clearly, the room-temperature thermopower S_{300K} is plotted in the inset of Fig. 5 as an example. As x increases, the value of S_{300K} increases monotonously from 122.6 μV/K (x = 0) to 166.2 μV/K (x = 0.4).

It is well-known that, in the strongly correlated $Ca_3Co_4O_9$ system, the almost T-independent larger thermopower at high temperatures can be expressed using the modified Heikes formula[29]:

$$S = -\frac{k_B}{e}\ln\left[\frac{g_3}{g_4}\left(\frac{y}{1-y}\right)\right] \quad (1)$$

where y is the Co^{4+} concentration, g_3 and g_4 are the spin-orbital degeneracy for Co^{3+} and Co^{4+} ions in CoO_2 layers. The X-ray absorption and photoemission spectroscopy studies have already shown that, in an undoped $Ca_3Co_4O_9$ sample, both Co^{3+} and Co^{4+} ions are in the low-spin (LS) states below ~350 K, g_3 and g_4 are 1 and 6, respectively.[30,31] From the analysis of both the resistive and magnetic data, the spin-state transition may not occur in the temperature range below ~350 K for these Ir-doped samples. Thus, for all studied samples, the LS states of both Co^{3+} and Co^{4+} ions are considered to be stable, and the spin-orbital degeneracy g_3 and g_4 keep 1 and 6 in these Ir-doped samples, respectively. Accordingly, the enhanced S is driven by the variation in the

concentration of Co^{4+} ions y according to Heikes formula. Based on the measured S, the value of y can be calculated and the results are shown in the inset of Fig. 5 as a function of Ir-doping level x. As x increases, the magnitude of y decreases monotonously, which are in agreement with the analysis of the carrier concentration estimated by Hall measurements.

Figure 6(a) shows the temperature dependence of the thermal conductivity κ for $Ca_3Co_{4-x}Ir_xO_9$ (x = 0, 0.1, 0.2, 0.3, and 0.4) samples. All samples show a similar $\kappa(T)$ behavior while κ decreases obviously via Ir doping. In general, the thermal conductivity in a material can be expressed by the sum of the phonon thermal conductivity κ_{ph} and the carrier thermal conductivity κ_{ch} as[32]:$\kappa = \kappa_{ph} + \kappa_{ch}$. The doped Ir ions with a larger ionic radius in the conductive CoO_2 layers can cause the disorder and the structural distortion as a point defect, and the induced lattice disharmony will scatter phonons and carriers. So the phonon and carrier transports will be suppressed and thus κ decrease obviously for the Ir-doped samples. The quantitative description of the thermal conductivity change can be seen clearly in Fig. 6(c), where the Ir-doping content dependence of the room-temperature thermal conductivity κ_{300K} is plotted as an example.

Using the measured ρ, S, and κ, we can calculate the dimensionless TE figure of merit ZT ($=S^2T/\rho\kappa$). The ZT value as a function of temperature for $Ca_3Co_{4-x}Ir_xO_9$ (x = 0, 0.1, 0.2, 0.3, and 0.4) samples is shown in Fig. 6(b). It can be seen that the value of ZT increases first and then decreases with increasing x. The ZT value of $Ca_3Co_{3.9}Ir_{0.1}O_9$ at room temperature reaches 0.0086, which is about 37% larger than that of $Ca_3Co_4O_9$ as shown in Fig. 6(d). The result shows that a proper Ir doping may be an effective route to improve the TE performance of $Ca_3Co_4O_9$ system.

(4) Magnetic Properties

The magnetic measurements of $Ca_3Co_{4-x}Ir_xO_9$ (x = 0, 0.1, 0.2, 0.3, and 0.4) samples were performed under zero-field-cooling (ZFC) and field-cooling (FC) modes at an applied magnetic field of 0.1 T. Both ZFC and FC susceptibility curves $\chi(T)$ for the x = 0.2 sample are shown in the main panel of Fig. 7(b) as an example. The FC $\chi(T)$ of all samples shows a Curie–Weiss paramagnetic behavior in the high-temperature range. As temperature decreases to ~19 K, FC $\chi(T)$ increases sharply, which is suggested to originate from the formation of the FIM state.[4,33] The ZFC $\chi(T)$ curves are more complicated. In the high-temperature range, Ir doping does not change the Curie–Weiss-like magnetic behavior of $\chi(T)$. However, as temperature decreases, there exists a distinctive separation between FC and ZFC $\chi(T)$ curves. ZFC $\chi(T)$ increases continually and reaches a maximum at a certain temperature (defined as the freezing temperature T_f), and then decreases rapidly in a limited temperature range of $T^{\delta} < T < T_f$. As the temperature decreases further, ZFC $\chi(T)$ increases again. That is to say, there exist a cusp at T_f and a valley at T^{δ} in the ZFC $\chi(T)$ curves for all samples. Similar magnetic behavior is also observed in $Ca_3Co_{4-x}Ti_xO_9$[15] and $Ca_3Co_{4-x}Cu_xO_9$[17] single crystals, which is usually considered to originate from the appearance of the spin-glass (SG) or cluster-glass state due to the competition between ferromagnetic (FM) and antiferromagnetic (AFM) exchange interactions.

Indeed, in $Ca_3Co_4O_9$ system, FIM interaction is the interlayer coupling interaction between Ca_2CoO_3 and CoO_2 layers, and both AFM and FM interactions are found within CoO_2 layers.[11] The glass state may be related to be the competition between FM and AFM exchange interactions within CoO_2 layers. As shown in the left insets of Fig. 7(b), FC susceptibility χ_{5K} at 5 K decreases obviously with increasing x, indicating the low-temperature FIM state can be well suppressed by Ir doping, which can also be further proved by the result of the magnetic-field-dependent magnetization $M(H)$ curves as shown in Fig. 7(a), where the data of the x = 0 and 0.3 samples are shown for examples. For the undoped sample, its $M(H)$ curve exhibits a clear hysteresis loop,

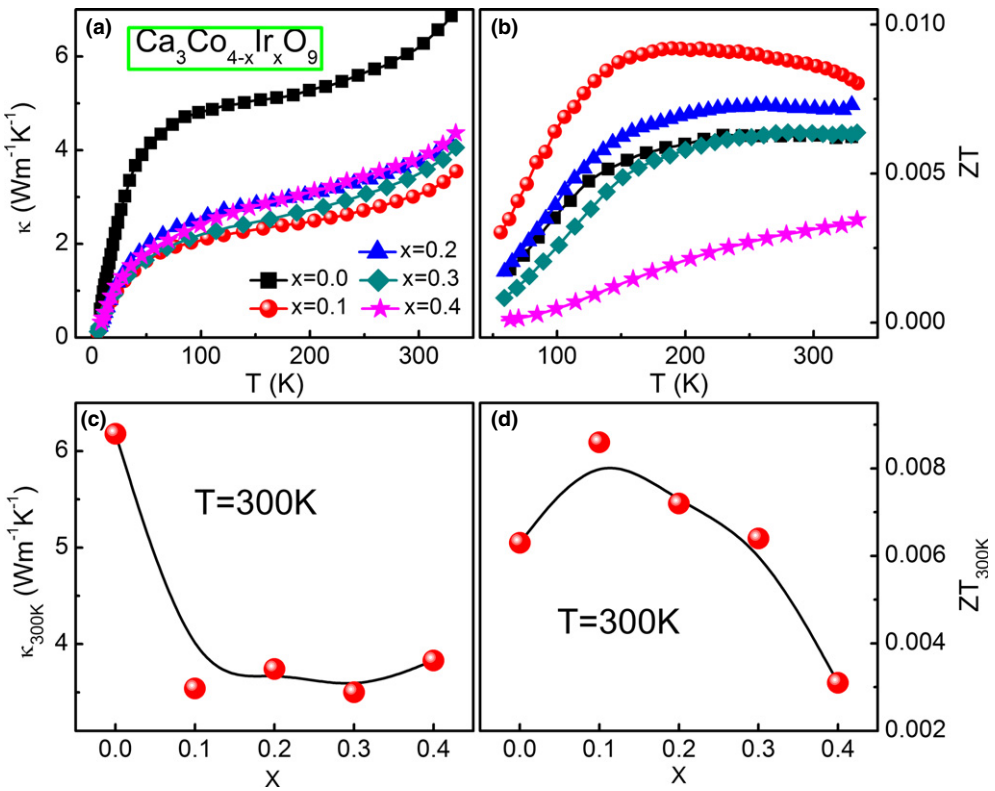

Fig. 6. Temperature dependences of (a) the thermal conductivity $\kappa(T)$ and (b) the dimensionless TE figure of merit $ZT(T)$ for $Ca_3Co_{4-x}Ir_xO_9$ (x = 0, 0.1, 0.2, 0.3, and 0.4); the room temperature (c) thermal conductivity κ_{300K} and (d) thermoelectric figure of merit ZT_{300K} as functions of Ir-doping level x.

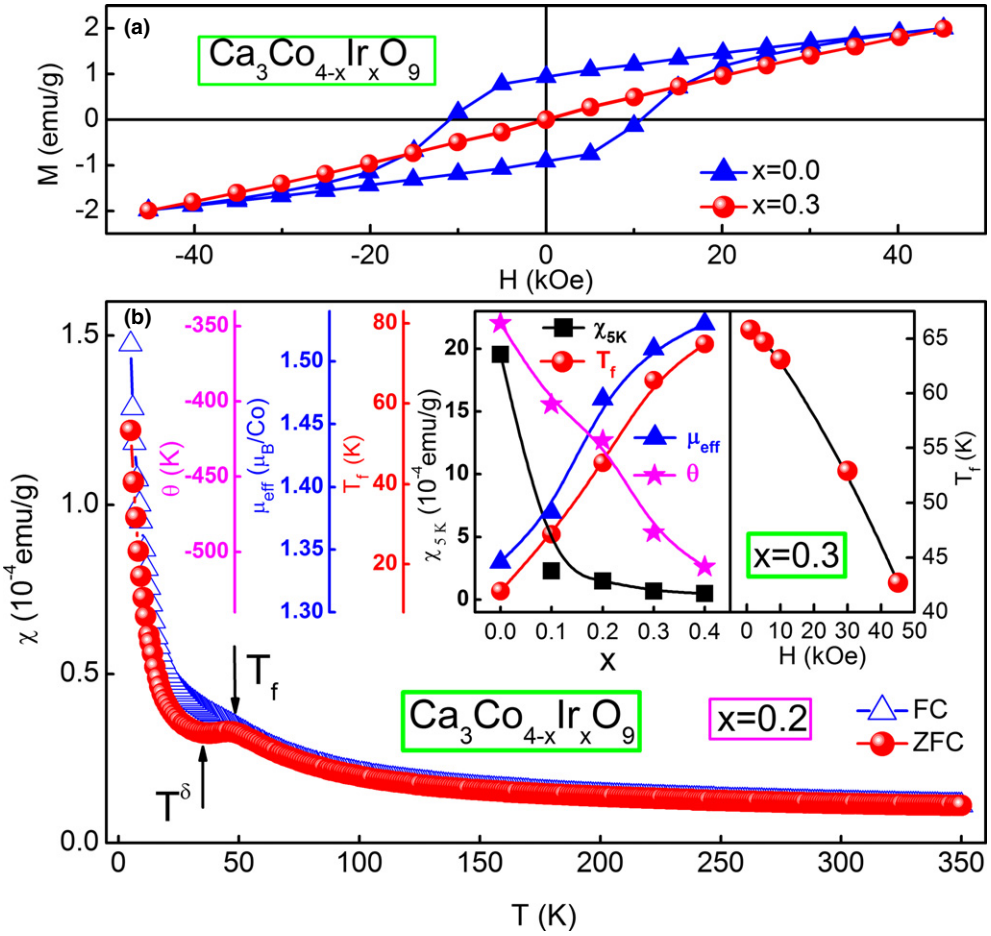

Fig. 7. (a) Relationship between M and H at 5 K for the $x = 0$ and 0.3 samples. (b) zero-field-cooling and field-cooling (FC) magnetic susceptibilities $\chi(T)$ as functions of temperature for the $x = 0.2$ sample, the left insets show the FC susceptibility at 5 K χ_{5K}, the freezing temperature T_f, the effective magnetic moment μ_{eff}, and the Weiss temperature θ as functions of Ir-doping content x, the right inset shows the freezing temperature T_f as a function of the applied magnetic field H for $Ca_3Co_{3.7}Ir_{0.3}O_9$.

whereas the hysteresis phenomenon is weakened obviously for all Ir-doped samples. The coercive field H_c decreases monotonously from 10.76 kOe for the $x = 0$ sample to 0.07 kOe for the $x = 0.4$ sample, indicating that the FIM interaction in this system has indeed been well suppressed by Ir doping. From the left inset of Fig. 7(b), one can also see that the value of T_f increases with increasing x. We performed the ZFC and FC $\chi(T)$ curves under the higher magnetic field H of 0.5, 1, 3, and 4.5 T for $Ca_3Co_{3.7}Ir_{0.3}O_9$ and the result is shown in the right inset of Fig. 7(b). With increasing H, the cusp around T_f in the ZFC $\chi(T)$ curve diminishes gradually and the value of T_f decreases monotonously, indicating the melting of the glass state.

To analyze quantitatively the effect of Ir doping on the magnetic properties, we try to fit the temperature dependence of the inverse FC susceptibility χ, i.e., $\chi^{-1}(T)$ according to the Curie–Weiss law: $\chi^{-1}(T) = 3k_B(T - \theta)N_0^{-1}\mu_{eff}^{-2}$, where θ, N_0, and μ_{eff} are Weiss temperature, Avogadro's constant, and effective magnetic moment, respectively.[14,15] The obtained fitting parameters θ and μ_{eff} are also plotted in the left inset of Fig. 7(b) against Ir-doping level x. In general, both Co^{3+} (LS, $s = 0$, $\mu_{eff} = 0\ \mu_B$) and Co^{4+} (LS, $s = 1/2$, $\mu_{eff} = 1.73\ \mu_B$) ions are in the LS state and Co^{2+} (HS, $s = 3/2$, $\mu_{eff} = 3.87\ \mu_B$) ions are in the high-spin (HS) state in $Ca_3Co_4O_9$ system at low temperatures.[34] Here, s is the quantum number of spin. The substitution of magnetic Ir^{4+} (LS, $s = 1/2$, $\mu_{eff} = 1.73\ \mu_B$) may decrease the relative concentration of Co^{4+} ions and increase that of Co^{2+} as discussed above. As a result, the average s and μ_{eff} increase as shown in the left inset of Fig. 7(b). As reported previously, superexchange and double exchange interactions coexist between Co^{3+} and Co^{4+} ions in $Ca_3Co_4O_9$ system.[14] The existence of AFM superexchange interaction at low temperatures in CoO_2 layers can be testified by the negative of θ in all studied samples. When partial Co ions are doped by Ir^{4+}, the absolute value of θ increases, indicating the reinforcement of the AFM superexchange interaction, which may lead to the enhancement of competition between FM and AFM exchanges within CoO_2 layers. It may be the reason that glass state appears at low temperatures and T_f increases with increasing x.

IV. Conclusion

In summary, the effects of Ir doping on the structural, electrical transport, thermal transport, and magnetic properties of $Ca_3Co_{4-x}Ir_xO_9$ ($x = 0$, 0.1, 0.2, 0.3, and 0.4) samples have been investigated systematically. Based on the analysis of XPS data, the valence state of the doped Ir ions is suggested to be +4. As Ir ions are doped into system, the resistivity and the MIT temperature increase monotonously with increasing x till to 0.3. The results indicate that Ir substitution with a larger ionic radius can enhance the carrier localization and result in more stable SDW state. For the $x = 0.4$ sample, the MIT disappears. The thermopower increases monotonously with increasing x due to the considerably decreased concentration of Co^{4+} ions. The room-temperature thermopower S_{300K} for the $x = 0.4$ sample reaches 166.2 μV/K, which is 36% larger than that of the undoped sample. The ZT value increases first and then decreases monotonously with increasing x. The maximal room-temperature ZT value for $Ca_3Co_{3.9}Ir_{0.1}O_9$ reaches 0.0086, which is about 37% larger

than that of $Ca_3Co_4O_9$. At the same time, Ir doping suppresses the low-temperature FIM state and also introduces a SG behavior at low temperatures.

Acknowledgments

This work is supported by the National Key Basic Research under contract no. 2011CBA00111, and the National Nature Science Foundation of China under contract nos. 11174293, U1232140, 11174288, and 10904151, and the Scientific Research Foundation for the Returned Overseas Chinese Scholar.

References

[1]M. Ito and D. Furumoto, "Effects of Mechanical and Ag Addition on Thermoelectric Properties of $Na_xCo_2O_9$," *Scripta Mater.*, **55** [6] 533, 4pp (2006).

[2]Y. Nishikubo, S. Nakano, K. Kudo, and M. Nohara, "Enhanced Thermoelectric Properties by Ir Doping of $PtSb_2$ with Pyrite Structure," *Appl. Phys. Lett.*, **100** [25] 252104, 3pp (2012).

[3]Y. N. Huang, B. C. Zhao, J. Fang, R. Ang, and Y. P. Sun, "Tunning of Microstructure and Thermoelectric Properties of $Ca_3Co_4O_9$ Ceramics by High-Magnetic-Field Sintering," *J. Appl. Phys.*, **110** [12] 123713, 13pp (2011).

[4]Y. Wang, Y. Sui, J. G. Cheng, X. J. Wang, W. H. Su, X. Y. Liu, and H. J. Fan, "Doping-Induced Metal-Insulator Transition and the Thermal Transport Properties in $Ca_{3-x}Y_xCo_4O_9$," *J. Phys. Chem. C*, **114** [11] 5174, 8pp (2010).

[5]I. Terasaki, Y. Sasago, and K. Uchinokura, "Large Thermoelectric Power in $NaCo_2O_4$ Single Crystals," *Phys. Rev. B*, **56** [20] R12685, 3pp (1997).

[6]A. C. Masset, C. Michel, A. Maignan, M. Hervieu, O. Toulemonde, F. Studer, B. Raveau, and J. Hejtmanek, "Misfit-Layered Cobaltite with an Anisotropic Giant Magnetoresistance: $Ca_3Co_4O_9$," *Phys. Rev. B*, **62** [1] 166, 10pp (2000).

[7]S. Li, R. Funahashi, L. Matsubara, K. Ueno, S. Sodeoka, and H. Yamada, "Synthesis and Thermoelectric Properties of the New Oxides Materials $Ca_{3-x}Bi_xCo_4O_{9+\delta}$ ($0.0 \le x \le 0.75$)," *Chem. Mater.*, **12** [8] 2424, 4pp (2000).

[8]R. Funahashi and M. Shikano, "$Bi_2Sr_2Co_2O_y$ Whiskers with High Thermoelectric Figure of Merit," *Appl. Phys. Lett.*, **81** [8] 1459, 3pp (2002).

[9]S. Hébert, S. Lambert, D. Pelloquin, and A. Maignan, "Large Thermopower in a Metallic Cobaltite: The Layered Tl-Sr-Co-O Misfit," *Phys. Rev. B*, **64** [17] 172101, 4pp (2001).

[10]Y. Wang, Y. Sui, P. Ren, L. Wang, X. J. Wang, W. H. Su, and H. J. Fan, "Strongly Correlated Properties and Enhanced Thermoelectric Response in $Ca_3Co_{4-x}M_xO_9$(M = Fe, Mn, and Cu)," *Chem. Mater.*, **22** [3] 1155, 9pp (2010).

[11]J. Soret and M. B. Lepetit, "Electronic Structure of the $Ca_3Co_4O_9$ Compound Fron *ab Initio* Local Interactions," *Phys. Rev. B*, **85** [16] 165145, 9pp (2012).

[12]S. Pinitsoontorn, N. Lerssongkram, A. Harnwunggmoung, K. Kurosaki, and S. Yamanaka, "Mechanical Synthesis, and Magnetic Properties of Transition Metals-Doped $Ca_3Co_{3.8}M_{0.2}O_9$," *J. Alloys Compd.*, **503** [2] 431, 5pp (2010).

[13]Y. Wang, L. X. Xu, Y. Sui, X. J. Wang, J. G. Cheng, and W. H. Su, "Enhanced Electron Correlation in Rare-Earth Doped $Ca_3Co_4O_9$," *Appl. Phys. Lett.*, **97** [6] 062114, 5pp (2010).

[14]B. C. Zhao, Y. P. Sun, W. J. Lu, X. B. Zhu, and W. H. Song, "Enhanced Spin Fluctuation in $Ca_3Co_{4-x}Ti_xO_9$ Single Crystals," *Phys. Rev. B*, **74** [14] 144417, 8pp (2006).

[15]B. C. Zhao, Y. P. Sun, and W. H. Song, "Magnetic and Transport Properties in the Ti Doped Cobaltite $Ca_3Co_{4-x}Ti_xO_9$ ($0 \le x \le 0.8$) Single Crystals," *J. Appl. Phys.*, **99** [7] 073906, 6pp (2006).

[16]S. Pinitsoontorn, N. Lerssongkram, N. Keawprak, and V. Amornkitbamrung, "Thermoelectric Properties of Transition Metals-Doped $Ca_3Co_{3.8}M_{0.2}O_{9+\delta}$ (M = Co, Cr, Fe, Ni, Cu and Zn)," *J. Mater. Sci.: Mater. Electron.*, **23** [5] 1050, 7pp (2012).

[17]Y. N. Huang, B. C. Zhao, X. B. Hu, S. Lin, R. Ang, W. H. Song, and Y. P. Sun, "Enhanced Electric Correlation and Thermoelectric Response by Cu-Doping in $Ca_3Co_4O_9$ Single Crystals," *Dalton Trans.*, **41**, 11176, 11pp (2012).

[18]M. Karppinen, H. Fjellvåg, T. Konno, Y. Morita, T. Motohashi, and H. Yamauchi, "Evidence for Oxygen Vacancies in Misfit-Layered Calcium Cobalt Oxide, $[CoCa_2O_3]_qCoO_2$," *Chem. Mater.*, **16** [14] 2790, 4pp (2004).

[19]X. G. Luo, X. H. Chen, G. Y. Wang, C. H. Wang, Y. M. Xiong, H. B. Song, and X. X. Lu, "The Evolution of Magnetotransport Properties with Carrier Concentration in $Ca_3Co_4O_{9+\delta}$ Single Crystals," *Europhys. Lett.*, **74** [3] 526, 7pp (2006).

[20]V. Petricek, M. Dusek, and L. Palatinus, *Jana2006. The Crystallographic Computing System*. Institute of Physics, Czech Republic, 2006.

[21]T. Wu, T. A. Tyson, H. Y. Chen, J. M. Bai, H. Wang, and C. Jaye, "A Structural Change in $Ca_3Co_4O_9$ Associated with Enhanced Thermoelectric Properties," *J. Phys. Condens. Matter*, **24** [45] 455602, 7pp (2012).

[22]Y. N. Huang, B. C. Zhao, R. Ang, S. Lin, Z. H. Huang, L. H. Yin, S. G. Tan, Y. Liu, W. H. Song, and Y. P. Sun, "Enhanced Electron Correlation in the In-Doped Misfited-Layered Cobaltite $Ca_3Co_4O_9$ Ceramics," *J. Am. Ceram. Soc.*, **96** [3] 791, 3pp (2013).

[23]C. D Ling, K. Aivazian, S. Schmid, and P. Jensen, "Structural Investigation of Oxygen Non-Stoichiometry and Cation Doping in Misfit-Layered Thermoelectric $(Ca_2CoO_{3-x})(CoO_2)_\delta$, $\delta \approx 1.61$," *J. Solid State Chem.*, **180** [4] 1446, 10pp (2007).

[24]T. Wu, T. Tyson, J. M. Bai, K. Pandya, C. Jaye, and D. A. Fischer, "On the Origin of Enhanced Thermoelectricity in Fe Doped $Ca_3Co_4O_9$," *J. Mater. Chem. C*, **1**, 4114, 7pp (2013).

[25]J. Sugiyama, H. Itahara, T. Tani, J. H. Brewer, and E. J. Ansaldo, "Magnetism of Layered Cobalt Oxides Investigated by Muon Spin Rotation and Relaxation," *Phys. Rev. B*, **66** [13] 134413, 9pp (2002).

[26]Y. N. Huang, B. C. Zhao, R. Ang, S. Lin, Z. H. Huang, S. G. Tan, Y. Liu, W. H. Song, and Y. P. Sun, "Enhanced Thermoelectric Performance and Room-Temperature Spin-State Transition of Co^{4+} Ions in the $Ca_3Co_{4-x}Rh_xO_9$ System," *J. Phys. Chem. C*, **117**, 11459, 12pp (2013).

[27]G. Yang, Q. Ramasse, and R. F. Klie, "Direct Measurement of Charge Transfer in Thermoelectric $Ca_3Co_4O_9$," *Phys. Rev. B*, **78** [15] 153109, 4pp (2008).

[28]Y. N. Huang, B. C. Zhao, R. Ang, S. Lin, W. H. Song, and Y. P. Sun, "Structure, Magnetic and Transport Properties in $Ca_3Co_{4-x}Sb_xO_9$ Ceramics," *J. Alloys Compd.*, **574** [15] 233, 7pp (2013).

[29]P. M. Chaikin and G. Beni, "Thermopower in the Correlated Hopping Regime," *Phys. Rev. B*, **13** [2] 647, 5pp (1976).

[30]Y. Wakisaka, S. Hirata, T. Mizokawa, Y. Suzuki, Y. Miyazaki, and T. Kajitani, "Electronic Structure of $Ca_3Co_4O_9$ Studied by Photoemission Spectroscopy: Phase Separation and Charge Localization," *Phys. Rev. B*, **78** [23] 235107, 6pp (2008).

[31]W. Koshibae, K. Tsutsui, and S. Maekawa, "Thermopower in Cobalt Oxides," *Phys. Rev. B*, **62** [11] 6869, 4pp (2000).

[32]Y. Wang, Y. Sui, X. J. Wang, W. H. Su, and X. Y. Liu, "Enhanced High Temperature Characteristics of Transition Metals Doped $Ca_3Co_4O_{9+\delta}$ by Cold High-Pressure Fabrication," *J. Appl. Phys.*, **107** [3] 033708, 9pp (2010).

[33]J. Sugiyama, J. H. Brewer, E. J. Ansaldo, H. Itahara, K. Dohmae, Y. Seno, C. Xia, and T. Tani, "Hidden Magnetic Transition in the Thermoelectric Layered Cobaltite $[Ca_2CoO_3]_{0.62}[CoO_2]$," *Phys. Rev. B*, **68** [13] 134423, 8pp (2003).

[34]A. Maignan, V. Caignaert, B. Raveau, D. Khomskii, and G. Sawatzky, "Thermoelectric Power of $HoBaCo_2O_{5.5}$: Possible Evidence of the Spin Blockade in Cobaltites," *Phys. Rev. Lett.*, **93** [2] 26401, 4pp (2004). □